Molecular Neurobiology (2019) 56:1653–1664
https://doi.org/10.1007/s12035-018-1182-x

Arginylated Calreticulin Increases Apoptotic Response Induced by Bortezomib in Glioma Cells

Andrea Comba[1] · Laura V. Bonnet[1] · Victor E. Goitea[1] · Marta E. Hallak[1] · Mauricio R. Galiano[1]

Received: 8 February 2018 / Accepted: 7 June 2018 / Published online: 18 June 2018

Abstract

After retrotranslocation from the endoplasmic reticulum to the cytoplasm, calreticulin is modified by the enzyme arginyltransferase-1 (ATE1). Cellular levels of arginylated calreticulin (R-CRT) are regulated in part by the proteasomal system. Under various stress conditions, R-CRT becomes associated with stress granules (SGs) or reaches the plasma membrane (PM), where it participates in pro-apoptotic signaling. The mechanisms underlying the resistance of tumor cells to apoptosis induced by specific drugs remain unclear. We evaluated the regulatory role of R-CRT in apoptosis of human glioma cell lines treated with the proteasome inhibitor bortezomib (BT). Two cell lines (HOG, MO59K) displaying distinctive susceptibility to apoptosis induction were studied further. BT efficiency was found to be correlated with a subcellular distribution of R-CRT. In MO59K (apoptosis-resistant), R-CRT was confined to SGs formed following BT treatment. In contrast, HOG (apoptosis-susceptible) treated with BT showed lower SG formation and higher levels of cytosolic and PM R-CRT. Increased R-CRT level was associated with enhanced mobilization of intracellular Ca^{2+} and with sustained apoptosis activation via upregulation of cell death receptor DR5. R-CRT overexpression in the cytoplasm of MO59K rendered the cells susceptible to BT-induced, DR5-mediated cell death. Our findings suggest that R-CRT plays an essential role in the effect of BT treatment on tumor cells and that ATE1 is a strong candidate target for future studies of cancer diagnosis and therapy.

Keywords Drug resistance · Apoptosis · Arginylated calreticulin · Arginyltransferase-1 · Glioma cells · Stress granules · Bortezomib

Abbreviations

SG	Stress granule
ATE1	Arginyltransferase-1
CRT	Calreticulin
R-CRT	Arginylated calreticulin
BT	Bortezomib
ER	Endoplasmic reticulum
PM	Plasma membrane
TRAIL	TNF-related apoptosis-inducing ligand
Fluo-3/AM	Fluo-3 acetoxymethyl ester

Andrea Comba and Laura V. Bonnet contributed equally to this work.

Electronic supplementary material The online version of this article (https://doi.org/10.1007/s12035-018-1182-x) contains supplementary material, which is available to authorized users.

✉ Mauricio R. Galiano
mgaliano@fcq.unc.edu.ar

[1] Facultad de Ciencias Químicas, Departamento de Química Biológica Ranwel Caputto, Centro de Investigaciones en Química Biológica de Córdoba (CIQUIBIC-CONICET), Universidad Nacional de Córdoba, 5000 Córdoba, Argentina

Introduction

Calreticulin (CRT) is a protein synthesized and coupled-translocated to the endoplasmic reticulum (ER), where it functions as a protein-folding chaperone and helps maintain calcium homeostasis [1]. We demonstrated previously that CRT, following retrotranslocation from the ER to the cytoplasm, is post-translationally arginylated by the enzyme arginyltransferase-1 (ATE1) in a calcium-dependent manner [2]. Arginylated CRT (R-CRT) content in the cytoplasm is regulated by the proteasomal system and is enhanced by inhibition of proteasomes [3]. Under various stress conditions, R-CRT may become associated with stress granules (SGs) [4] or localized at the plasma membrane (PM) [5], where it plays a regulatory role in cell survival. Membrane exposure of the non-arginylated form of CRT has been proposed as a biomarker for cancer diagnosis [6]. However, a possible association of R-CRT with carcinogenic processes in mammalian cells has not been systematically studied.

Arginylation of CRT is not essential for its membrane exposure; however, we showed that R-CRT functions more efficiently as a pre-apoptotic signaling molecule than does non-

arginylated CRT [5]. We also observed that both non-arginylated CRT and R-CRT are targets of proteasomes in the cytoplasm, but that half-life of non-arginylated CRT is shorter than that of R-CRT [3], suggesting that arginylation enhances the stability of CRT protein. Similarly, Saha's group showed that ATE1 activity is necessary to stabilize mRNA levels of HSP40 and HSP70 during heat stress response [7]. ATE1 activity in eukaryotic cells also plays an essential role in the control of DNA mutagenesis through induction of growth arrest and/or cell death under various stress conditions [8]. Accordingly, *ATE1* expression was proposed to help control metastatic processes through tumor-suppressive activity [9]. These findings, and the observed increase of R-CRT under stress conditions [2–5], suggest R-CRT as a candidate molecular link in the modulation of cancer cell death susceptibility.

Gliomas, the most common type of human primary brain tumor, are highly aggressive and resistant to cell death induction [10–12]. The resistance of gliomas and other solid tumors to cell death induction by treatment with the proteasome inhibitor bortezomib (BT) is associated in part with the capability of tumor cells to form cytosolic SGs [13–15]. In view of the correlation between resistance to BT and formation of SGs, and our findings that cytosolic R-CRT is a component of SGs or is relocated to PM, we hypothesize that post-translational arginylation of CRT is a novel biological regulator of cancer cell death induction. In the present study, we evaluated the role of R-CRT in glioma cell death resulting from BT treatment. Cytosolic accumulation of R-CRT during BT treatment was associated with efficient cell death of human oligodendroglioma HOG via extrinsic caspase-3/DR5. Our findings suggest that cell death in BT-treated cells is regulated in part by R-CRT expression and localization and that further investigation of the function of R-CRT as apoptosis promoter will have useful clinical applications.

Experimental Procedures

Cell Lines and Culture Conditions

Human glioma cell lines MO59K, LN-229, and T98G were from the American Type Culture Collection (ATCC; Manassas, VA, USA). Human oligodendroglioma cell line HOG was kindly provided by Dr. M. Zakin (Unité d'Expression des Genes Eucaryotes, Pasteur Institute, Paris, France). Mouse EF (embryonic fibroblast) cell lines $ATE1^{+/+}$ and $ATE1^{-/-}$ were kindly provided by Dr. Anna Kashina (University of Pennsylvania, Philadelphia, PA, USA). All cells were grown in a humidified incubator (5% CO_2 atmosphere) with high-glucose DMEM (Invitrogen; Grand Island, NY, USA), containing 4.5 g/l glucose, 4 mM L-glutamine, and 25 mmol/l HEPES, supplemented with 1 mM sodium pyruvate, 0.25 μg/ml amphotericin B (Sigma-Aldrich; St. Louis, MO, USA), 200 units/ml penicillin, 100 μg/ml streptomycin (Invitrogen), and 10% heat-inactivated FBS (Invitrogen), as described previously [3]. Cell line stocks were maintained with < 20 passages. The absence of mycoplasma was tested and confirmed periodically by specific PCR and by DNA immunofluorescence staining with Hoechst 0.5 μg/ml (B115 bisBenzimide H33258). Proteasome inhibitor BT (Selleckchem; Houston, TX, USA) was dissolved in DMSO vehicle at initial dilution 2 μM for treatment of cells.

Cell Viability Assay

Cell viability was determined by a colorimetric/fluorometric technique using resazurin (Sigma-Aldrich) as described previously [16]. For each assay, cells were placed on 96-well plates (5000 cells/well) and cultured in a standard medium. Next day, the cells were treated with various concentrations of BT (10, 100, 500, 1000, 2000 nM) or corresponding vehicle (control) in 200 μl medium. Twenty-four hours later, each well was added with 2 μl resazurin solution (1 mg/ml). Plates were incubated 4 h at 37 °C, and fluorescent signal was measured (wavelength 560 nm excitation/590 nm emission) in a GloMax-Multi Detection System Microplate Reader (Promega; Madison, WI, USA).

Apoptosis Assay

Redistribution of phosphatidylserine (an apoptosis marker) in PM was assessed using phycoerythrin (PE)-conjugated Annexin V (BD Biosciences; Carlsbad, CA, USA) as per the manufacturer's protocol. Cells (60,000) were seeded on a 24-well plate, treated, collected, washed with PBS, pelleted, and resuspended in binding buffer (10 mM HEPES/NaOH (pH 7.4), 40 mM NaCl, 2.5 mM $CaCl_2$) containing 1% PE-conjugated Annexin V and 1% fluorescent dye 7-amino-actinomycin D (7-AAD) to identify dead cells. Samples were kept in the dark and incubated for 15 min prior to flow cytometric analysis on a FACSCanto II cytometer using FACSDiva software program (BD Biosciences). Apoptosis was also determined by immunofluorescence assay using cleaved caspase-3 antibody (Cell Signaling) as per the manufacturer's protocol. Images were obtained with an AxioPlan epifluorescence microscope (Carl Zeiss AG; Oberkochen, Germany).

Immunofluorescence

Cells were grown to 60% confluence on glass coverslips in 24-well plates as described previously [4]. Cells were then treated with BT, placed on ice, washed with PBS, fixed with 4% paraformaldehyde-PBS (pH 7.2) for 20 min at 4 °C, permeabilized with 0.1% Triton X-100 for 10 min, and washed 3× with PBS. Non-specific binding sites were blocked

with 5% BSA in PBS for 1 h at room temperature. Cells were incubated with primary antibodies (rabbit anti-R-CRT and goat anti-TIA-1 (T cell intracytoplasmic antigen 1; SG marker) (Santa Cruz Biotechnology; Dallas, TX, USA); mouse anti-DR5 (TRAIL-R2) pAb (eBioscience; San Diego, CA, USA)), washed 3× with PBS, and incubated for 1 h with respective secondary antibody (Alexa Fluor 546-conjugated goat anti-rabbit IgG; Alexa Fluor 488-conjugated donkey anti-goat IgG; Alexa Fluor 488-conjugated goat anti-mouse IgG in PBS) (Thermo Fisher Scientific, Rockford, IL, USA). The nuclei were stained with DAPI. Images were acquired with a laser scanning confocal microscope (model FluoView 1000, Olympus; Center Valley, PA, USA) with a × 60 oil immersion lens, NA 1.42. Fiji software program (http://fiji.sc) was used to evaluate SG formation, measure cell fluorescence, and calculate corrected total cell fluorescence (CTCF) with correction for background fluorescence. Colocalization was analyzed using Fiji Colocalization Finder Plugin.

Flow Cytometric Analysis of Cell Surface and Intracellular Proteins

R-CRT and DR5 exposure on the cell surface and total intracellular levels of R-CRT and caspase-3 following BT treatment were assessed by flow cytometry. In brief, 7×10^5 cells were plated on 60-mm dishes and treated the next day with BT at various concentrations and durations. Both adherent and detached cells were harvested, washed 2× with cold PBS, and fixed with 0.25% paraformaldehyde for 10 min on ice. For intracellular staining, cells were then permeabilized with 0.01% Triton X-100 for 10 min, washed 3× with PBS, incubated for 1 h at 4 °C with primary antibodies in cold PBS, washed, incubated with corresponding mouse or rabbit IgG antibody conjugated to 488 and/or Cy5 (1:500) (Thermo Fisher) for 1 h, and analyzed by FACSCanto II cytometer. Isotype-matched IgG antibodies were used as controls. A total of 100,000 cells were counted for each point. Data were recorded on a logarithmic scale and analyzed using FACSDiva.

Proteasomal Activity Assay

MO59K and HOG cells were treated 24 h with MG132 (10 μM), BT (500 nM), or no treatment (control), trypsinized, and washed 2× with cold PBS. Cell lysates were prepared by sonication in the buffer containing 50 mM Tris-HCl (pH 7.5), 5 mM $MgCl_2$, 2 mM ATP, 0.5 mM EDTA, 250 mM sucrose, and 1 mM DTT. Protein concentration was determined by Bradford assay. Chymotrypsin-like activity of proteasomes was determined by hydrolysis of fluorogenic substrate suc-LLVY-AMC. Protein (7 μg) from cleared lysates was incubated with 100 mM suc-LLVY-AMC in 200 μl reaction buffer (50 mM Tris-HCl (pH 7.5), 40 mM KCl, 5 mM $MgCl_2$, 0.5 mM ATP, 1 mM DTT) for 1 h at 37 °C, and the reaction was stopped by the addition of 500 μl 5% SDS. Fluorescence readings of released 7-amido-4-methyl-coumarin (AMC) were measured (wavelength 380 nm excitation/460 nm emission) in a FluoroMax-P spectrofluorometer system (HORIBA Jobin Yvon; Edison, NJ, USA).

Plasmids and Transfection

MO59K and ATE1$^{-/-}$ cells were plated in Opti-MEM medium (Invitrogen) and transfected 24 h later with expression vector encoding Ub-fused mature human R-CRT pEGFP-Ub-R-CRT or control vector pEGFPC146A as described previously [3], using Lipofectamine LTX with Plus reagent (Thermo Fisher) for 6 h, as per the manufacturer's protocol. Twenty-four hours after transfection, cells were treated with BT or control vehicle for various durations as indicated.

Real-Time Reverse Transcription PCR

Total RNA was extracted from cultured cells using TRIzol reagent (Invitrogen). ImProm-IIReverse Transcriptase (Promega; Madison, WI, USA) was used to reverse-transcribe 5 μg RNA. A portion of total cDNA was amplified by RT-PCR using Mezcla Real SYBR Green (Biodynamics S.R.L., CAB, Argentina) and the following primer sets: hDR4: sense ACCTTCAAGTTTGTCGTCGTC, antisense CCAAAGGGCTATGTTCCCATT; hDR5: sense ACAGTTGCAGCCGTAGTCTTG, antisense CCAGGTCG TTGTGAGCTTCT; and h18S: sense CGGTACAG TGAAACTGCGAA, antisense CCGTCGGCATGTAT TAGCTC. Amplification was performed using Rotor-Gene Q (Qiagen; Foster City, CA, USA). Each RNA level was normalized relative to corresponding housekeeping RNA level in the same sample. Data were calculated by the 2ΔCt method.

Immunoblotting

Western blotting analysis was performed as described previously [2]. Cells (1.5×10^6) were plated in standard medium with 10% FBS and subjected to treatment or transfection experiments 24 h later. Cells were lysed with RIPA buffer plus protease inhibitor cocktail (Invitrogen), separated by SDS-PAGE, and transferred onto nitrocellulose membrane. Primary antibodies used were mouse anti-CRT mAb (BD Biosciences) and rabbit anti-R-CRT pAb (custom-made by Eurogentec; Seraing, Belgium; specifically detects R-CRT) [2], mouse anti-ATE1 mAb (SCBT; Dallas, TX, USA), and mouse anti-polyubiquitinylated conjugates (Enzo Life Sciences; Farmingdale, NY, USA). Secondary antibodies used were IRDye 800CW goat anti-mouse and IRDye 650CW goat anti-rabbit antibody (LI-COR Biosciences; Lincoln, NE,

USA), with visualization by Odyssey infrared imaging system (LI-COR). Samples were normalized relative to equal amounts of β-actin (Sigma-Aldrich). Band intensities were quantified using ImageJ software program.

Measurement of Intracellular Calcium (Ca^{2+}) Concentration

HOG and MO59K cells (5×10^4) were plated on 6-well Nunc Lab-Tek chambered coverglass (Thermo Fisher) and treated with BT or control vehicle for various durations. Intracellular Ca^{2+} concentration was quantified using fluorescent Ca^{2+} dye indicator Fluo-3 acetoxymethyl ester (Fluo-3/AM) (Thermo Fisher). In brief, cells were washed with medium without FBS and loaded with Fluo-3/AM (5 μM) and pluronic F-127 acid (0.2%, *w*/*v*) for 30 min at 37 °C. Ca^{2+} was measured by exciting the indicator (range 450–500 nm) every 30 s, for 10 min. Images of cells were obtained using a laser confocal microscope (model FV1000, Olympus) connected to a 37 °C/5% CO_2 atmosphere chamber, with UPLFLN × 40, NA 1.3 Plan-Apochromat objective. Pinholes were set for nominal axial resolution < 0.6 μm. Excitation was produced by a 25-mW argon laser emitting at 488 nm, and emissions were collected using a 505–530-nm band-pass filter for Alexa Fluor 488. Normalized values of the relative fold change of fluorescence (Ft-Fo/Fo) of each cell were analyzed at 6 or 24 h of BT treatment. Relative fold change of Ca^{2+} fluorescence intensity was plotted as a function of time for each treatment condition. Fluorescence intensity was quantified using an image analysis system (FLUOVIEW 1.7 software program).

Statistical Analysis

Differences among experimental groups were evaluated using ANOVA models followed by Duncan's test for mean comparisons (significance criterion $p < 0.05$ or < 0.01). Experiments were performed in triplicate and repeated at least 3×, unless otherwise noted. Statistical analyses were performed using InfoStat 2016 software program (Grupo InfoStat, Universidad Nacional de Córdoba; Córdoba, Argentina).

Results

Variable Cell Death Susceptibility of Human Glioma Cells to BT Treatment

The drug bortezomib (BT), a selective inhibitor of the 26S proteasome, is highly efficient for the treatment of multiple myeloma and mantle cell lymphoma [17]. On the other hand, various cell lines derived from solid tumors are resistant to BT treatment [18–21]. We evaluated the effects of BT treatment on the viability of human glioma cell lines MO59K, LN-229, T98G, and HOG. In general, BT caused dose-dependent reduction of viability, and susceptibility of the four cell lines to BT treatment varied significantly. HOG was more susceptible than MO59K, with reduced viability (IC50) at BT concentration 100 nM. MO59K (glioblastoma-derived) was more resistant to BT than HOG, with reduced viability at 1000 nM, up to 2000 nM, no IC50 was achieved (Suppl. Fig. 1a). We observed that BT strongly inhibited proteasomal activity in both HOG and MO59K (Suppl. Fig. 1b) and therefore used these two cell lines for further experiments. The possible relationship between BT effects on cell viability and apoptotic cell death events was evaluated by flow cytometric analysis with Annexin V and 7-AAD following 24 h drug treatment. Consistently with cell viability assay results, HOG, in comparison with MO59K, showed a significantly higher dose-dependent increase in apoptotic cell percentage, larger populations of early and late apoptotic cells, and smaller populations of viable cells (Fig. 1a, b). Caspase-3 activation was assessed by immunofluorescence, as a complement to cell death analysis. BT treatment of HOG induced significant increases of cleaved caspase-3 at concentrations 500 and 100 nM after 6 and 24 h treatment, respectively. Under the same conditions, MO59K showed no increase of cleaved caspase-3 (Fig. 1c; Suppl. Fig. 1c). In conclusion, BT had

Fig. 1 Differential effect of BT treatment on caspase-3-dependent cell death induction and SG formation in glioma-derived cell lines HOG and MO59K. **a** Percentages of apoptotic cells were analyzed by flow cytometry following binding to PE-conjugated Annexin V and 7-AAD. One hundred percent values correspond to 50,000 cells. Values shown are mean ± SE; $n = 3$. **b** Representative flow cytometry dot plots of cells treated as in **a**. Early apoptosis cells (PE-Annexin V+/7-AAD−), late apoptosis and dead cells (PE-Annexin V+/7-AAD+) and (PE-Annexin V−/7-AAD+), and viable cells (PE-Annexin V−/7-AAD−) are indicated respectively as Q1, Q2, Q3, and Q4. Results indicate greater apoptosis induction in HOG than in MO59K. **c** Immunofluorescence assay of relative percentages of positive cleaved caspase-3 cells after 6 and 24 h BT treatment. Apoptosis was estimated as number of positive cleaved caspase-3/total nuclei per visual field. Values shown are mean ± SE from ≥ 10 fields of each condition, randomly selected for counting (blinded manner) in two independent experiments. $*p < 0.01$ for comparison with control group (DMSO). **d** Percentages of SG-containing cells were estimated in confocal images (× 60; 1600 × 1600 pixels). Values shown are mean ± SE from ≥ 50 cells analyzed per condition in two independent experiments. SG formation was correlated with resistance to BT-induced cell death. **e** Cells treated with control vehicle (DMSO) or BT (500 nM) for 24 h were analyzed by double immunofluorescence using anti-R-CRT pAb and anti-TIA-1 (SG marker) pAb. Unprocessed confocal images (× 60, 1600 × 1600 pixels) were analyzed using Fiji ImageJ Colocalization Finder Plugin. Insets represent a zoomed portion of merged images. Scatterplot (lower panel) shows the combinations of intensities from both channels in SG pixels present in control and BT-treated MO59K images. A co-localization profile corresponding to BT-treated MO59K image was analyzed along cross-section (white line) of green and red color intensities. Pearson's correlation coefficient values (*r*) was determined from selected images indicate BT-induced colocalization of R-CRT with TIA-1 (SGs) in MO59K. Results shown are from one experiment representative of two independent experiments. Scale bars = 20 μm; inset scale bars = 2 μm

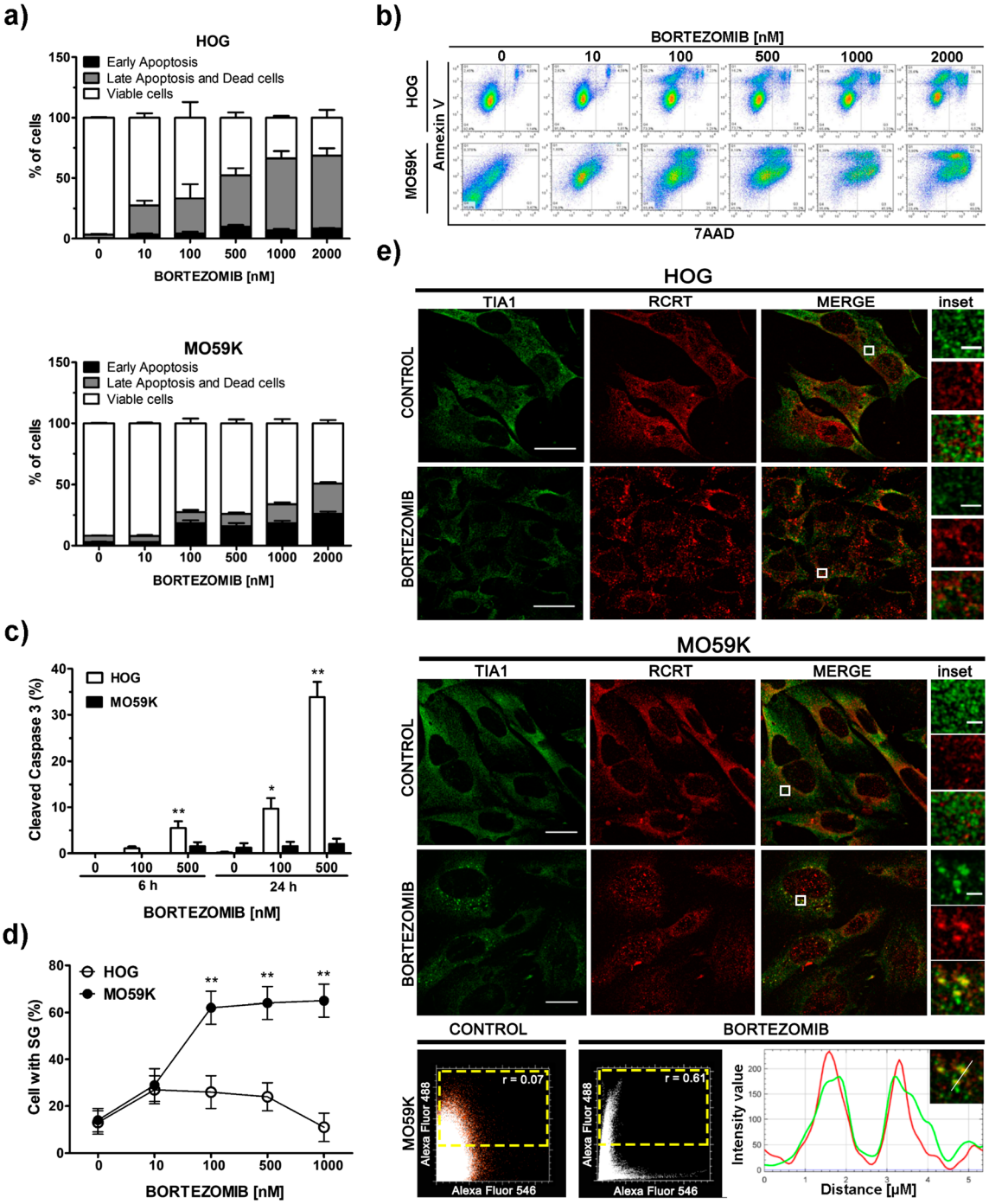

differential effects on cell death induction among the tested cell lines; HOG was most susceptible and MO59K was most resistant to BT treatment. Caspase-3 activation was involved in BT-induced cell death.

Induction of SG Formation and Association of R-CRT with SGs in BT-Resistant Cells

SG formation in tumor cells has been shown to be correlated with resistance to chemotherapeutic agents such as BT [13–15]. We further evaluated the effect of BT on glioma cell lines by assessing SG formation in HOG (most susceptible) and MO59K (most resistant). SG formation was estimated by immunofluorescence using anti-TIA1 (SG marker) antibody following 24 h treatment with BT at various concentrations (Fig. 1d, e; Suppl. Fig. 1d). MO59K showed significant increases in the percentage of SG-forming cells (Fig. 1d) and in number of SGs per cell (Fig. 1e; Suppl. Fig. 1d). In contrast, HOG showed reduced SG formation, consistent with its greater

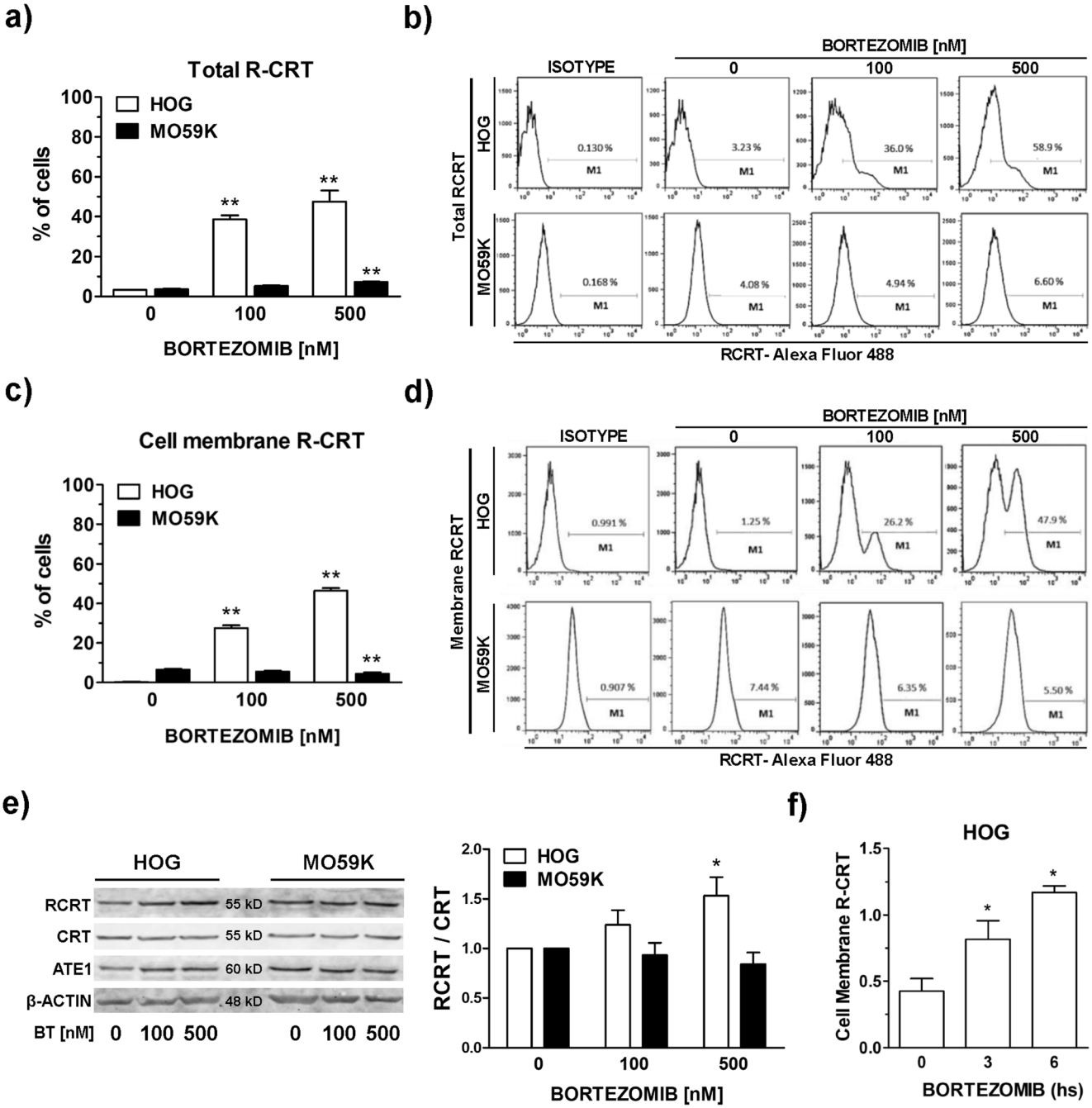

Fig. 2 R-CRT enhancement and PM exposure are associated with apoptosis induction following BT treatment. HOG and MO59K were treated with control vehicle (DMSO) or BT (100 and 500 nM) for 24 h. **a** Triton-permeabilized and **c** non-permeabilized cells were immunostained with anti-R-CRT pAb and analyzed by flow cytometry. Background fluorescence signals were determined from unstained cells and cells incubated with secondary antibody (Alexa Fluor 488) alone (isotype control). Positive signal was defined as fluorescence greater than that observed for secondary antibody alone. One hundred percent values correspond to 100,000 cells for each point. Values shown are mean ± SE from three independent experiments. *$p < 0.05$; **$p < 0.01$ vs. control. **b**, **d** Representative flow cytometry histograms showing percentage of cells positive for intracellular and membrane R-CRT, respectively, gated within a marker (M1). Isotype control: background fluorescence signal of cells without primary antibody. Results shown are from one experiment representative of three independent experiments. **e** After 24-h BT treatment, cells were lysed and analyzed by Western blotting with anti-R-CRT, anti-CRT, anti-ATE1 antibodies, and anti-β-actin (loading control) (left panel). Quantification of representative immunoblots of R-CRT/CRT ratio (right panel) shows the increase of arginylated protein following treatment in HOG vs. MO59K. Error bars represent SE from three different experiments. PM R-CRT expressed as fluorescence intensity of HOG cells analyzed by flow cytometry with anti-R-CRT pAb after 0 (control), 3 and 6 h of BT treatment. Background fluorescence signals were determined from unstained cells and cells incubated with secondary antibody alone. Positive signal was defined as fluorescence greater than that observed for secondary antibody alone. Values shown are mean ± SE from three independent experiments. *$p < 0.05$

susceptibility to BT treatment. SG formation was evaluated at various time points. HOG showed a notable reduction of SG formation even at 30-min BT treatment, as well as at 1, 3, and 6 h. MO59K showed consistently higher SG formation, with a maximum at 24 h (Suppl. Fig. 1e).

We previously observed an association of R-CRT with SGs in cells treated with stressors such as sodium arsenite and thapsigargin-EDTA [2, 4]. A possible relationship between R-CRT and BT-induced SG formation in MO59K was assessed by confocal microscopy in the present study, and a strong association was observed after 24 h (Fig. 1e). Pearson's colocalization coefficient was increased in BT-treated MO59K (Fig. 1e, lower panel). These findings indicate that SG formation and SG-associated R-CRT patterns in BT-treated glioma cells are correlated with differential susceptibility to apoptosis.

Increase of R-CRT Level and R-CRT Exposure on PM Are Correlated with Apoptosis Induction Following BT Treatment

In view of our previous finding that stressors such as sodium arsenite enhance R-CRT level and R-CRT exposure on PM in apoptotic cells [5], we performed flow cytometric analysis of these parameters in HOG and MO59-K under short and long BT treatment. Intracellular R-CRT level was notably increased in HOG but not in MO59-K (Fig. 2a, b). Similarly, PM exposure of R-CRT was increased in HOG but reduced in MO59-K (Fig. 2c, d). Immunoblotting analysis revealed a significant increase of R-CRT level in HOG, that is not observed in MO59K (Fig. 2e). These increased R-CRT levels were not due to increased CRT expression, of CRT, since BT treatment does not affect CRT levels (Fig. 2e); rather, BT treatment increased arginylation of CRT. In contrast, BT treatment had no effect on ATE1 expression in either HOG or MO59-K (Fig. 2e).

Because BT efficiently inhibits proteasomal activity in both HOG and MO59K (Suppl. Fig. 1b), the relatively higher levels of R-CRT in HOG following BT treatment are presumably related to some other effect of BT. We treated the two cell lines with BT for 3 and 6 h to determine whether the enhancement of R-CRT level in PM occurs earlier than apoptosis induction. After 3 h BT treatment, HOG (but not MO59K) showed a sustained increase of R-CRT in PM (Fig. 2f). These findings suggest that post-translational arginylation of CRT is enhanced in HOG and that R-CRT exposed on PM following BT treatment functions as a pro-apoptotic protein to trigger programmed cell death, consistent with the results of our previous study [5].

BT Increases Alteration of Ca^{2+} Homeostasis and Promotes Apoptosis in HOG

Various candidate molecular pathways potentially account for the differential responses of MO59K and HOG to BT treatment. We showed previously that CRT is retrotranslocated from the ER to the cytoplasm, where it undergoes post-translational arginylation under stress conditions that affect Ca^{2+} homeostasis [2, 4]. We examined the possibility that differential responses of the two cell lines to BT treatment are related to alterations of intracellular Ca^{2+} levels. Analysis of Ca^{2+} mobilization using Fluo-3/AM dye revealed an increase of intracellular Ca^{2+} in BT-treated HOG, but not MO59K (Fig. 3a). This finding was consistent with the higher R-CRT levels observed in HOG vs. MO59K (Fig. 2a–e). Relative fold change of fluorescence assessed in both cell lines showed a small reduction of Ca^{2+} levels during the time monitored (10 min) after 6 h of BT treatment (Supplem. Fig. 2a). However, HOG cells that showed increased Ca^{2+} levels after 24 h of BT treatment (Fig. 3a) maintain a growing bent of Ca^{2+} levels during 10 min of calcium analysis (Supplem. Fig. 2b). This tendency of Ca^{2+} levels is not observed in MO59K at the same time of treatment (Supplem. Fig. 2b) and correlates with the scare change of Ca^{2+} mobilization determined in MO59K following BT treatment. Such effect also correlates with unchanged R-CRT expression (Fig. 2a, e) that appeared to be strongly associated with SGs in these cells after treatment (Fig. 1e), similar to the previous studies of cells exposed to different stressors [3, 4].

To bypass the effect of BT on calcium storage in BT-resistant MO59K, we performed transient transfections to overexpress Ub-R-CRT-EGFP in the cytoplasm. Such R-CRT overexpression in the cytoplasm reduced cell viability (Fig. 3b) and increased apoptosis (Fig. 3c, d) following BT treatment, rendering the cells BT-susceptible.

BT-Induced Cell Death Is Modulated by ATE1 and its Product R-CRT

R-CRT level was enhanced in cells in which caspase-3-dependent apoptosis was induced by BT treatment (Fig. 2a–e). Because CRT is post-translationally modified by ATE1 during BT treatment, we examined the role of R-CRT and ATE1 (the enzyme responsible for CRT arginylation) in the regulation of this apoptotic process. BT cytotoxicity in ATE1-expressing ($ATE1^{+/+}$) and ATE1 knockout ($ATE1^{-/-}$) cells was evaluated to assess the dependence of BT effect on protein arginylation. After 24-h BT treatment, cell viability was reduced to a much greater degree in $ATE1^{+/+}$ than in $ATE1^{-/-}$ (Fig. 4a). Assay of apoptosis parameters by flow cytometry with Annexin V and 7-

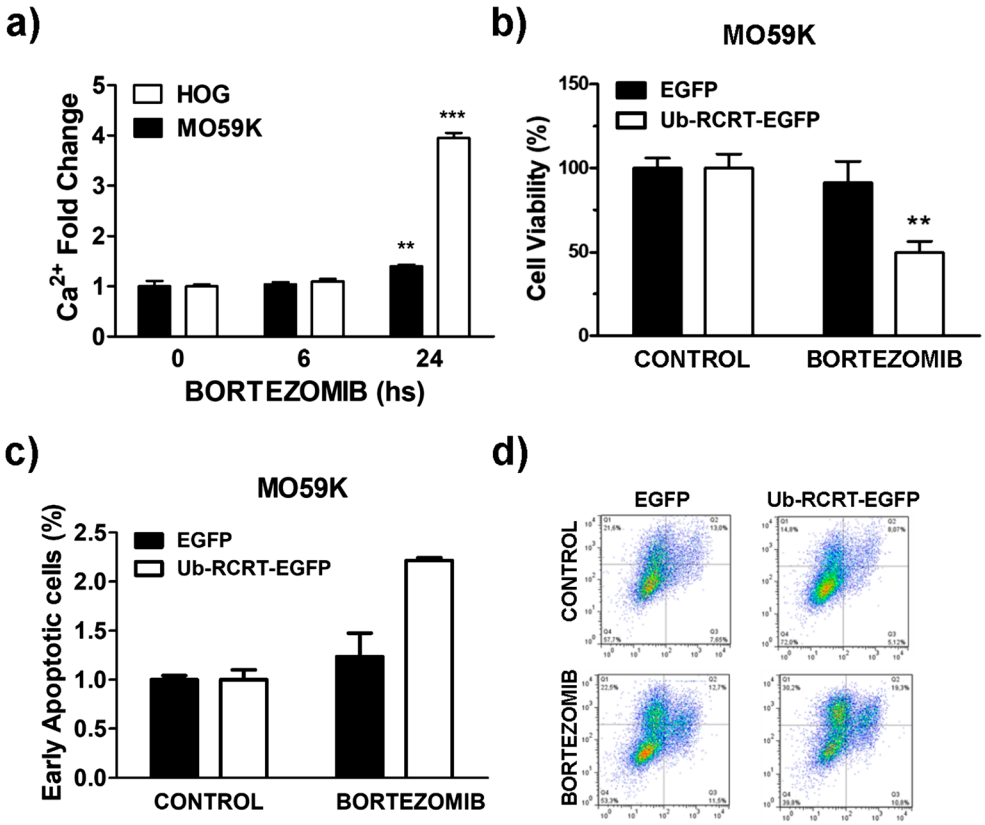

Fig. 3 BT-induced apoptosis is correlated with enhanced Ca^{2+} mobilization and post-translational arginylation of CRT. **a** HOG and MO59K were treated with BT (500 nM) or control vehicle (DMSO) for 6 and 24 h. Intracellular Ca^{2+} concentration was quantified as described in experimental procedures. Normalized values of the relative fold change of fluorescence (Ft-Fo/Fo) of each cell were determined at 6 or 24 h of BT treatment for each cell line. Values shown are mean ± SE; $n = 19$–57 cells (HOG), 35–45 cells (MO59K). ***$p < 0.0001$, **$p < 0.001$ vs. control group (DMSO). **b**–**d** MO59K were transfected with Ub-RCRT-EGFP for R-CRT overexpression in cytosol or with control vector. After 12 h, cells were treated with control vehicle (DMSO) or BT (100 nM) for 24 h. **b** Cell viability was assayed using fluorometric indicator dye resazurin. Values shown are mean ± SE; $n = 3$. **$p < 0.01$ vs. control. **c** Analysis of early cell apoptosis percentage by flow cytometry using PE-Annexin V and 7-AAD binding. One hundred percent values correspond to 50,000 cells. Values shown are mean ± SE; $n = 3$. *$p < 0.05$ vs. control. **d** Representative flow cytometry dot plots of MO59K cells treated as in **c**, with notations Q1, Q2, Q3, and Q4 as defined for Fig. 1b

AAD in cells treated with 100 or 500 nM BT for 24 h showed a significantly greater increase of early and late apoptosis induction levels in $ATE1^{+/+}$ than in $ATE1^{-/-}$ (Fig. 4b, c). Similarly, the percentage of positive cleaved caspase-3 induced by BT treatment showed a significantly greater increase in $ATE1^{+/+}$ than in $ATE1^{-/-}$ (Fig. 4d). A possible role of R-CRT in this process was assessed by overexpressing R-CRT in the cytoplasm of $ATE1^{-/-}$ cells. R-CRT overexpression per se significantly reduced the viability of transfected cells relative to control (EGFP+) cells, consistent with our previous findings [5]. R-CRT-overexpressing cells were also more susceptible to BT treatment, resulting in a greater decrease of viability (Fig. 4e). These findings indicate that the cytotoxic effects of BT are modulated by ATE1 activity through CRT arginylation.

Cell Death Receptor DR5 Is Involved in Activation of R-CRT-Regulated Apoptosis

We next considered the question of which apoptosis signaling pathway is used by R-CRT to exert its effect on BT-treated cells. BT and other proteasome inhibitors were previously shown to activate extrinsic apoptosis signaling pathway involving transmembrane receptors TRAIL-R1 (DR4) and TRAIL-R2 (DR5) in tumor cells [22, 23]. We evaluated mRNA expression of cell death receptors DR4 and DR5 in HOG and MO59K by RT-PCR assay. Twenty-four-hour BT treatment significantly increased DR5 mRNA level in HOG but not in MO59K (Fig. 5a). This treatment also increased DR4 mRNA in HOG, but to a lesser degree than that of DR5 mRNA (Suppl. Fig. 2c).

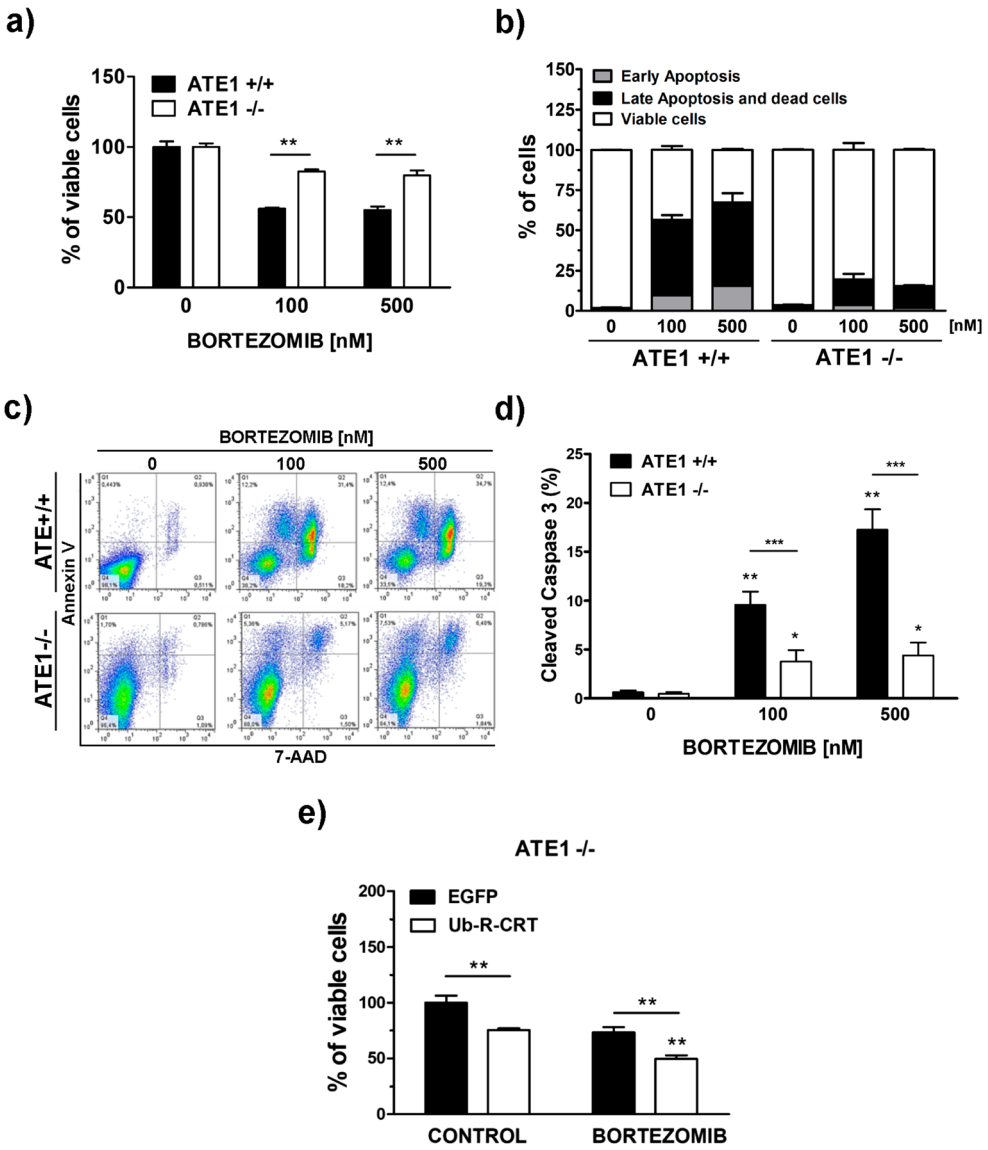

Fig. 4 R-CRT regulates BT-induced cell death. **a** Cell viability was assessed by resazurin assay for ATE1$^{+/+}$ and ATE1$^{-/-}$ cells treated with BT (100 and 500 nM) for 24 h. Values shown are mean ± SE; $n = 3$. $^{**}p < 0.01$ vs. control. **b** ATE1$^{+/+}$ and ATE1$^{-/-}$ were treated with BT as in **a**, and apoptosis was determined by flow cytometry using PE-Annexin V and 7-AAD. **c** Representative flow cytometry dot plots of apoptosis analysis in **b**. **d** Expression of cleaved caspase-3 in ATE1$^{+/+}$ and ATE1$^{-/-}$ was analyzed by immunofluorescence after 24 h treatment with BT (100 and 500 nM) or DMSO. Apoptosis percentage was estimated as number of positive cleaved caspase-3/total nuclei per visual field. Values shown are mean ± SE from ≥ 10 fields of each condition, randomly selected for counting (blinded manner) in two independent experiments. $^{*}p < 0.05$; $^{**}p < 0.01$ vs. control. $^{***}p < 0.01$, ATE1$^{+/+}$ vs. ATE1$^{-/-}$. **e** ATE1$^{-/-}$ were transfected with Ub-RCRT-EGFP for R-CRT overexpression in cytosol or with control vector. After 12 h, cells were treated with BT (500 nM) for 24 h, and cell viability was assayed using resazurin as in **a**

DR5 protein expression levels in PM were evaluated by flow cytometry. After 24-h BT treatment, DR5 expression was greatly increased in HOG, whereas that in MO59K was increased temporarily but became indistinguishable from control level by 24 h (Fig. 5b, c). Evaluation of DR5 protein expression by immunofluorescence assay showed that DR5 PM exposure in HOG was strongly increased by 24 h treatment with 100 or 500 nM BT (Fig. 5d). R-CRT overexpression in MO59K, which increased the susceptibility of this BT-resistant cell line to apoptosis (Fig. 4c, d), also increased DR5 level in PM (Fig. 5e). These findings suggest that increased R-CRT level is part of a novel DR5-based cell death induction pathway.

Discussion

The proteasome inhibitor bortezomib (BT) is a chemotherapeutic drug used in the treatment of various types of human cancer. It displays relatively low effectiveness against solid tumors, such as gliomas, which are characterized by high resistance to cell death induction [15]. Results of the present study indicate that resistance to BT treatment is modulated by arginylated calreticulin (R-CRT). Insertion of R-CRT into PM of glioma cells undergoing BT treatment results in activation of apoptotic signals. Susceptibility of glioma cell lines to BT treatment was strongly correlated with expression and subcellular localization of R-CRT. BT-resistant cell line

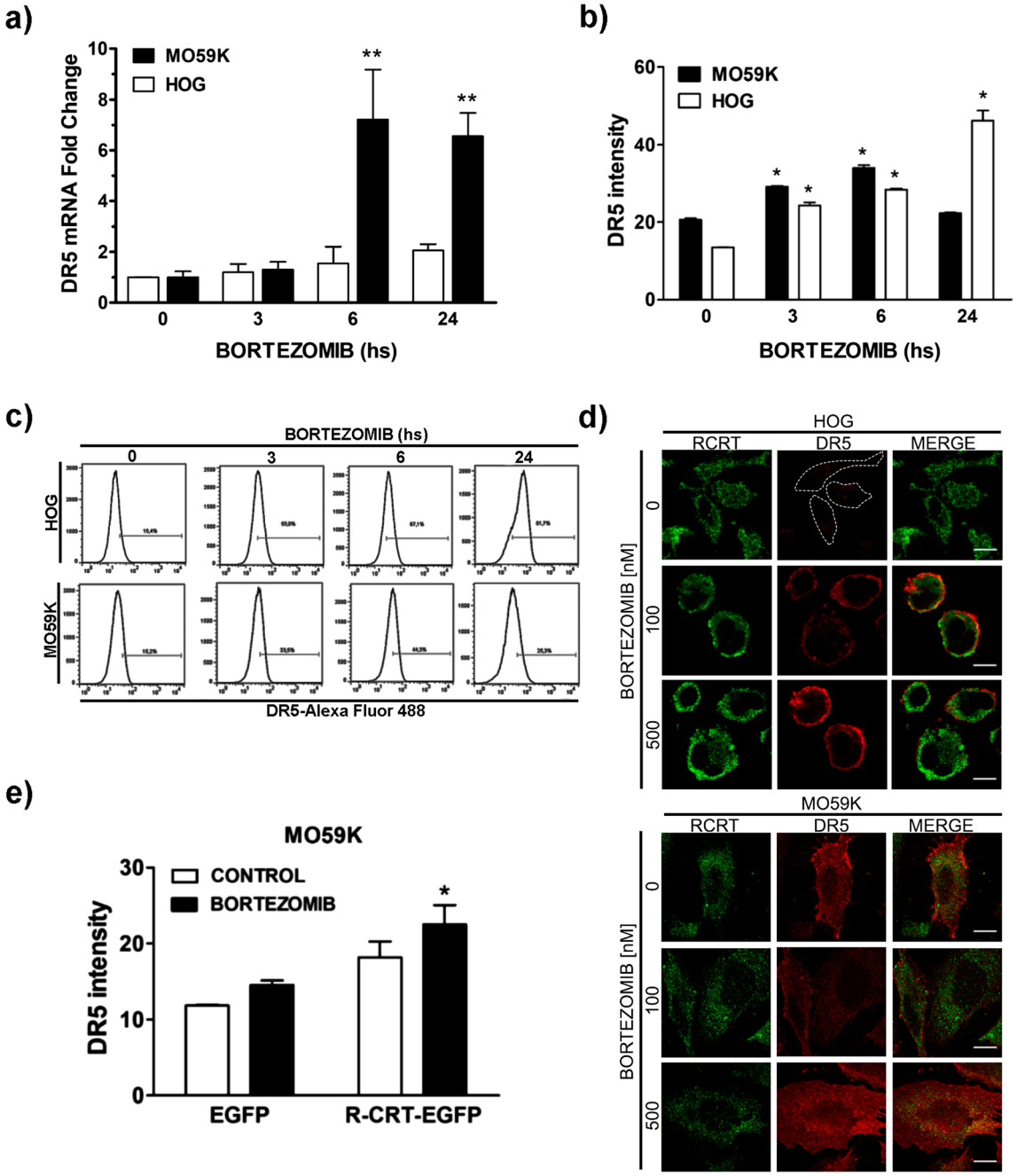

Fig. 5 Cell death receptor DR5 is involved in the activation of R-CRT-mediated apoptosis. **a** DR5 mRNA expression levels were determined by RT-PCR in HOG and MO59K treated with BT (500 nM) for 3, 6, or 24 h. Values shown are mean ± SE; $n = 3$. $^{**}p < 0.01$ vs. control (DMSO). **b** PM expression of DR5 was analyzed by flow cytometry using anti-DR5 primary antibody and Alexa Fluor 488-conjugated secondary antibody in cells treated as in **a**. One hundred percent values correspond to 100,000 cells for each point. Values shown are mean ± SE; $n = 3$. $^{*}p < 0.05$ vs. control (DMSO). **c** Representative flow cytometry histograms showing percentage of cells positive for membrane DR5 gated within a marker (R1). Isotype control: background fluorescence signal of cells without primary antibody. Results shown are from one experiment representative of three independent experiments. **d** PM expression of DR5 determined by immunofluorescence using anti-DR5 primary antibody and Alexa Fluor 546-conjugated secondary antibody. Nuclei were stained with DAPI. Cell morphology was outlined (white dot line) in DR5 staining of HOG control condition. Representative confocal images (× 60, 1600 × 1600 pixels) are shown. Scale bars = 10 μm. **e** MO59K cells were transfected with Ub-R-CRT-GFP expression vector or control vector for 24 h and then treated with BT (100 nM) for 24 h. Left panel: membrane expression of DR5 was analyzed by flow cytometry using anti-DR5 primary antibody and Cy5 secondary antibody for GFP-positive populations. Unstained, non-transfected cells, cells transfected with GFP alone, and cells stained with secondary antibody alone were used as controls for the determination of background fluorescence signal and for channel compensation. One hundred percent values correspond to 100,000 cells for each point. Values shown are mean ± SE; $n = 3$. $^{*}p < 0.05$ vs. control

MO59K displayed strong induction of SG formation and association of R-CRT with these dynamic structures. Previous studies suggest that SG formation is a resistance response of cancer cells to certain types of drugs, including proteasome inhibitors [13, 14]. Sequestration of R-CRT in cytoplasmic SGs as we observed in BT-treated cells, and associated resistance to apoptosis, is consistent with the results of prior studies indicating that mechanisms of cell death resistance involve sequestration of pro-apoptotic proteins in these transient cytoplasmic components [13–15, 24]. R-CRT was strongly associated with SGs in BT-treated MO59K (Fig. 1e), suggesting that resistant cells have a distinct assembly of SGs that facilitates the recruitment of the arginylated protein. In contrast, inhibition of proteasomes by BT in BT-susceptible HOG altered ER homeostasis, facilitating arginylation of CRT; however, these cells did not efficiently form SGs containing R-CRT (Fig. 1e; Suppl. Fig. 1d, e).

HOG displayed strong induction of CRT arginylation and translocation of this post-translationally modified protein to PM, where it was involved in the induction of apoptotic events. Such apoptosis induction by R-CRT involved activation of caspase-3 signaling. We demonstrated similarly in a previous study that under certain stress conditions (e.g., prolonged sodium arsenite treatment), R-CRT is transferred to PM and functions as a pro-apoptotic protein [5]. Studies by other groups have revealed direct association of CRT membrane exposure with apoptotic processes, including immunogenic cell death [25–28]; however, no such association has been shown for R-CRT.

Increased R-CRT levels rendered cells more susceptible to apoptosis induction through DR5 receptor activation, which mediates extrinsic apoptotic pathway. Similarly, treatment of glioma cell lines with BT alone was shown to enhance resistance to cell death, while this effect was reversed by the activation of DR5 receptor through co-administration of soluble TRAIL ligand [29]. Treatment of cancer cells with carfilzomib, another proteasome inhibitor, induced apoptosis through overexpression and activation of extrinsic DR5 apoptosis signaling [30].

The association we observed between increased arginylation of CRT by ATE1 and apoptosis induction in BT-treated glioma cells is consistent with recent reports identifying ATE1 activity as a potential therapeutic target for suppression of cancer development. ATE1 exerts tumor suppressor activity that helps modulate cell death, angiogenesis induction, motility, and metastasis of tumor cells [8, 9]. In the present study, cytosolic overexpression of R-CRT in MO59K overcame resistance to BT-induced apoptosis (i.e., cells became susceptible to BT), suggesting that R-CRT is a key molecule in BT-induced cell death. Such a role of R-CRT was also supported by our finding that susceptibility to BT was lower in ATE1$^{-/-}$ than in ATE1$^{+/+}$ fibroblasts (Fig. 4a–d). R-CRT overexpression in ATE1$^{-/-}$ increased BT susceptibility (Fig. 4e), similar to the findings in MO59K.

R-CRT overexpression in the cytoplasm of ATE1$^{-/-}$ cells increased their susceptibility to apoptosis induction upon BT treatment. However, we cannot rule out the possibility that ATE1 modifies some other proteins involved in cellular responses to BT.

In summary, we observed distinctive responses to BT treatment in four cell lines derived from gliomas with differing degrees of malignancy. As part of such responses, R-CRT may undergo distinctive subcellular localization, which is correlated with their susceptibility to apoptosis induction upon BT treatment. Based on our findings, we propose that R-CRT exposure in PM may serve as a novel prognostic marker for glioma treatment and that strategies designed to promote R-CRT expression and its localization in PM will contribute to improved cancer treatments. Our findings also suggest that the enzyme ATE1 is a strong candidate target for future studies of cancer diagnosis and therapy.

Acknowledgements This study was supported by grants from the Agencia Nacional de Promoción Científica y Tecnológica (BID 2015 PICT-3655); Consejo Nacional de Ciencia y Tecnología, Argentina; and Secretaria de Ciencia y Tecnología de la Universidad Nacional de Córdoba, Argentina, to Marta Hallak and Mauricio Galiano. Andrea Comba was a postdoctoral fellow of CONICET. Laura Bonnet is a fellow at FONCYT. The authors are grateful to Dr. S. Anderson for the English editing of the manuscript. The authors thank Dr. C. Mas, Dr. C. Sampedro, Ms. S. Deza, Ms. G. Schachener, and Dr. Guillermo Pilar for the technical assistance and helpful advice.

Compliance with Ethical Standards

Conflict of Interest The authors declare that they have no conflict of interest.

References

1. Wang WA, Groenendyk J, Michalak M (2012) Calreticulin signaling in health and disease. Int J Biochem Cell Biol 44:842–846
2. Decca MB, Carpio MA, Bosc C, Galiano MR, Job D, Andrieux A, Hallak ME (2007) Post-translational arginylation of calreticulin: a new isospecies of calreticulin component of stress granules. J Biol Chem 282:8237–8245
3. Goitea VE, Hallak ME (2015) Calreticulin and arginylated calreticulin have different susceptibilities to proteasomal degradation. J Biol Chem 290:16403–16414
4. Carpio MA, Lopez Sambrooks C, Durand ES, Hallak ME (2010) The arginylation-dependent association of calreticulin with stress granules is regulated by calcium. Biochem J 429:63–72
5. Lopez Sambrooks C, Carpio MA, Hallak ME (2012) Arginylated calreticulin at plasma membrane increases susceptibility of cells to apoptosis. J Biol Chem 287:22043–22054
6. Liu R, Gong J, Chen J, Li Q, Song C, Zhang J, Li Y, Liu Z et al (2012) Calreticulin as a potential diagnostic biomarker for lung cancer. Cancer Immunol Immunother : CII 61:855–864

7. Deka K, Singh A, Chakraborty S, Mukhopadhyay R, Saha S (2016) Protein arginylation regulates cellular stress response by stabilizing HSP70 and HSP40 transcripts. Cell Death Discovery 2:16074
8. Kumar A, Birnbaum MD, Patel DM, Morgan WM, Singh J, Barrientos A, Zhang F (2016) Posttranslational arginylation enzyme Ate1 affects DNA mutagenesis by regulating stress response. Cell Death Dis 7:e2378
9. Rai R, Zhang F, Colavita K, Leu NA, Kurosaka S, Kumar A, Birnbaum MD, Győrffy B et al (2016) Arginyltransferase suppresses cell tumorigenic potential and inversely correlates with metastases in human cancers. Oncogene 35:4058–4068
10. Stewart LA (2002) Chemotherapy in adult high-grade glioma: a systematic review and meta-analysis of individual patient data from 12 randomised trials. Lancet 359:1011–1018
11. Stupp R, Mason WP, van den Bent MJ, Weller M et al (2005) European Organisation for, T. Treatment of Cancer brain, G. Radiotherapy, G. National Cancer Institute of Canada Clinical Trials, radiotherapy plus concomitant and adjuvant temozolomide for glioblastoma. N Engl J Med 352:987–996
12. Bao S, Wu Q, McLendon RE, Hao Y, Shi Q, Hjelmeland AB, Dewhirst MW, Bigner DD et al (2006) Glioma stem cells promote radioresistance by preferential activation of the DNA damage response. Nature 444:756–760
13. Fournier MJ, Gareau C, Mazroui R (2010) The chemotherapeutic agent bortezomib induces the formation of stress granules. Cancer Cell Int 10:12
14. Gareau C, Fournier MJ, Filion C, Coudert L, Martel D, Labelle Y, Mazroui R (2011) p21(WAF1/CIP1) upregulation through the stress granule-associated protein CUGBP1 confers resistance to bortezomib-mediated apoptosis. PLoS One 6:e20254
15. Vilas-Boas Fde A, da Silva AM, de Sousa LP, Lima KM et al (2016) Impairment of stress granule assembly via inhibition of the eIF2alpha phosphorylation sensitizes glioma cells to chemotherapeutic agents. J Neuro-Oncol 127:253–260
16. Comba A, Almada LL, Tolosa EJ, Iguchi E, Marks DL, Vara Messler M, Silva R, Fernandez-Barrena MG et al (2016) Nuclear factor of activated T cells-dependent down-regulation of the transcription factor glioma-associated protein 1 (GLI1) underlies the growth inhibitory properties of arachidonic acid. J Biol Chem 291:1933–1947
17. Richardson P (2003) Clinical update: proteasome inhibitors in hematologic malignancies. Cancer Treat Rev 29(Suppl 1):33–39
18. Adams J, Palombella VJ, Sausville EA, Johnson J, Destree A, Lazarus DD, Maas J, Pien CS et al (1999) Proteasome inhibitors: a novel class of potent and effective antitumor agents. Cancer Res 59:2615–2622
19. Yin D, Zhou H, Kumagai T, Liu G, Ong JM, Black KL, Koeffler HP (2005) Proteasome inhibitor PS-341 causes cell growth arrest and apoptosis in human glioblastoma multiforme (GBM). Oncogene 24:344–354
20. Styczynski J, Olszewska-Slonina D, Kolodziej B, Napieraj M, Wysocki M (2006) Activity of bortezomib in glioblastoma. Anticancer Res 26:4499–4503
21. McConkey DJ, Zhu K (2008) Mechanisms of proteasome inhibitor action and resistance in cancer, drug resistance updates: reviews and commentaries in antimicrobial and anticancer. Chemotherapy 11: 164–179
22. Liu X, Yue P, Chen S, Hu L, Lonial S, Khuri FR, Sun SY (2007) The proteasome inhibitor PS-341 (bortezomib) up-regulates DR5 expression leading to induction of apoptosis and enhancement of TRAIL-induced apoptosis despite up-regulation of c-FLIP and survivin expression in human NSCLC cells. Cancer Res 67:4981–4988
23. Jane EP, Premkumar DR, Pollack IF (2011) Bortezomib sensitizes malignant human glioma cells to TRAIL, mediated by inhibition of the NF-{kappa}B signaling pathway. Mol Cancer Ther 10:198–208
24. Mazroui R, Di Marco S, Kaufman RJ, Gallouzi IE (2007) Inhibition of the ubiquitin-proteasome system induces stress granule formation. Mol Biol Cell 18:2603–2618
25. Obeid M, Tesniere A, Ghiringhelli F, Fimia GM, Apetoh L, Perfettini JL, Castedo M, Mignot G et al (2007) Calreticulin exposure dictates the immunogenicity of cancer cell death. Nat Med 13: 54–61
26. Tufi R, Panaretakis T, Bianchi K, Criollo A, Fazi B, di Sano F, Tesniere A, Kepp O et al (2008) Reduction of endoplasmic reticulum Ca^{2+} levels favors plasma membrane surface exposure of calreticulin. Cell Death Differ 15:274–282
27. Wiersma VR, Michalak M, Abdullah TM, Bremer E, Eggleton P (2015) Mechanisms of translocation of ER chaperones to the cell surface and immunomodulatory roles in cancer and autoimmunity. Front Oncol 5:7
28. Panaretakis T, Kepp O, Brockmeier U, Tesniere A, Bjorklund AC, Chapman DC, Durchschlag M, Joza N et al (2009) Mechanisms of pre-apoptotic calreticulin exposure in immunogenic cell death. EMBO J 28:578–590
29. Balyasnikova IV, Ferguson SD, Han Y, Liu F, Lesniak MS (2011) Therapeutic effect of neural stem cells expressing TRAIL and bortezomib in mice with glioma xenografts. Cancer Lett 310:148–159
30. Han B, Yao W, Oh YT, Tong JS, Li S, Deng J, Yue P, Khuri FR et al (2015) The novel proteasome inhibitor carfilzomib activates and enhances extrinsic apoptosis involving stabilization of death receptor 5. Oncotarget 6:17532–17542